KnE Materials Science

MIE-2017
15th International School-Conference "New materials – Materials of innovative energy development, characterization methods and application''
Volume 2018

Knowledge E
Engaging minds

Conference Paper

Heating Kinetics Simulation During Spark-Plasma Sintering of Non-Conductive Materials

Nikita Rubinkovskiy and Anatoly Zholnin

National Research Nuclear University MEPhI (Moscow Engineering Physics Institute), Kashirskoe shosse 31, Moscow, 115409, Russia

Abstract

The simulation of aluminum oxide spark-plasma sintering has been carried out during this research, namely the temperature field distribution in the sample volume and mold at different heating phases. The research work was based on experimental data on the measurement of temperature on the matrix surface, in its hole and various internal parts, including the punches, in the absence of thermal insulating felt. It was experimentally discovered that the key source of heat release up to temperatures 1300-1400 °C is the contact resistance at the matrix punch boundaries. Then the heat dissipation zone moves towards the punches. The collected data helped to figure out thermal and electrical parameters for the materials used in the die mold. They provided a good coincidence of the observed and calculated figures of heat distribution at different temperatures. The parameters helped to calculate the temperature fields in the die molds with heat-insulating felts.

Keywords: spark-plasma sintering, finite element modeling, temperature distribution, electric and thermal contact.

Corresponding Author:
Nikita Rubinkovskiy
fissium@yandex.ru

Received: 21 December 2017
Accepted: 15 April 2018
Published: 6 May 2018

Publishing services provided by Knowledge E

Selection and Peer-review under the responsibility of the MIE-2017 Conference Committee.

1. INTRODUCTION

Spark-plasma sintering (SPS) is one of the promising methods of ceramic material consolidation [1-4]. The SPS principle is that pulsed direct current and mechanical pressure jointly effect on the powder material. Material in the affected area is heated to very high temperatures. Powder spark-plasma sintering is performed in a conductive graphite die-mold, therefore, this technology is unlimited for different types of sintered powder materials. When conductive powders are sintered, heating of the powders and the resulting compacts is carried out by direct passage of a current through them, while sintering of non-conductive materials - by the mold graphite element heating.

Along with all the SPS advantages there is a serious disadvantage: in installations where the sample temperature is controlled by measuring of the mold surface or the

hole temperature made in it, it is not possible to figure exact temperature of the sample itself. This fact can lead to underheating, overheating or uneven heating of the sintered material, which will affect the final properties of the compact in turn.

SPS has very wide possibilities for various powder sintering and great technological process flexibility, the result of which depends on a large number of different parameters. This significantly complicates the appointment of rational technological modes. In addition, the lack of objective knowledge about the processes taking place in the powder backfill when SPS limits the technology theoretical description level, and, accordingly, the predictive abilities of existing theories. The empirical approach continues to be the key method for SPS research and development of technological processes of material creation. However, the high cost and laboriousness of such experiments determine the need for the application of methods of numerical modeling and the further development of the theoretical description of SPS.

Most models are limited to only the horizontal thermoelectric contacts [5-7]. However, the vertical contact resistances are much bigger than the horizontal ones, which is shown in [8, 9, 15]. Some researches take into account the mechanical pressure influence on the distribution of temperature fields during sintering [10-15]. The difficulty of the process modeling is also that it is difficult to value each parameter effect separately [16].

The main purpose of this research was to simulate spark-plasma sintering of aluminum oxide, taking into account the effect of contact resistances, namely the distribution of temperature fields in the volume of the sample and the mold at different stages of heating in order to take into account possible errors in the production of finished products, i.e. temperature measurements for various materials with different geometry of compacts.

2. MATERIALS AND METHODS

Standard experiments on spark-plasma sintering were performed using an aluminum oxide tablet on a LABOX ^{TM} Model 625 (Sinter Land, Japan), the scheme of which is presented in Fig. 1.

The installation consists of a graphite matrix (height 30 mm, external diameter 35 mm, internal diameter 15.4 mm) into which the previously sintered sample is put in, two graphite punches (height 20 mm, diameter 15 mm), graphite spacer systems of various diameters (60 and 90 mm) and a height of 15 mm, as well as water-cooled electrodes brought to the lower and upper spacers.

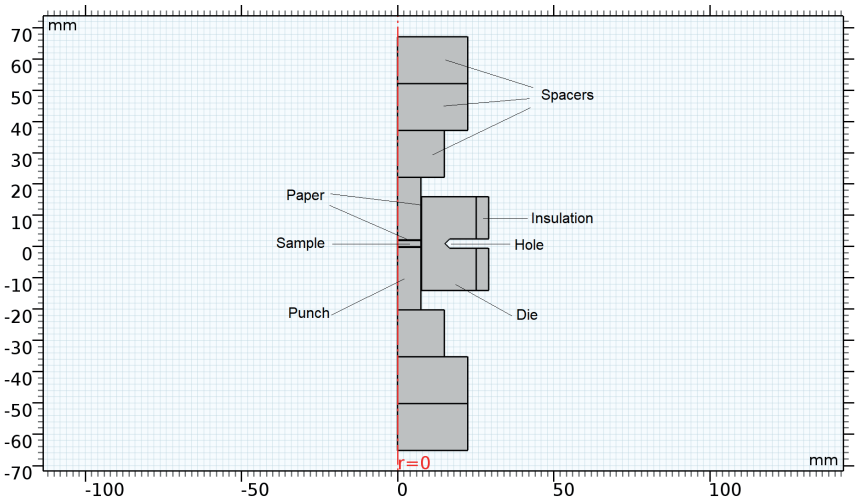

Figure 1: Scheme of spark-plasma sintering installation in axial symmetry.

At the boundaries of the punch-matrix, the punch-sample, and also the sample-matrix a graphite paper 0.2 mm thick was placed. The matrix was surrounded by heat-insulating graphite felt in order to reduce heat loss due to radiation.

Temperature measurements were carried out using an optical pyrometer measuring 573 - 3000 °C, focused in a 5 mm diameter matrix hole. The adjustment of the electric current was performed in an automatic mode by means of a PID controller. Temperature measurements on different surfaces of the system were carried out without heat-insulating felt. The mold photos were made using a digital camera.

The simulation was performed using the finite element method with the usage of COMSOL Multiphysics®. In solving of the thermoelectric problem, the basic equations were the heat conduction equation with the heat release function and the electric field equations describing the electric current passage through the material. The problem was considered in an axisymmetric formulation, where the temperature T (r, z, t) is a function of the time t and of the cylindrical coordinates z and r [17]:

$$\rho C_p \frac{\partial T}{\partial t} = \frac{1}{r}\frac{\partial}{\partial r}\left(rk_r\frac{\partial T}{\partial r}\right) + \frac{1}{z}\frac{\partial}{\partial z}\left(rk_z\frac{\partial T}{\partial z}\right) + q_i, \quad (1)$$

where ρ is the density, k_r and k_z are coefficients of the thermal conductivity in r and z directions, respectively, c_p is the specific heat, q_i is the heat generated by the Joule heating per unit of volume per unit of time.

The properties for the materials used in the calculation were taken from the researches [18, 19].

The current distribution is calculated by the following equation:

$$\frac{1}{r}\frac{\partial\left(ri_r\right)}{\partial r} + \frac{\partial i_z}{\partial z} = 0, \quad (2)$$

where i_r и i_z – the current density in the r and z directions, respectively.

The electrical potential was applied to the upper spacer, the potential on the lower spacer was equal to zero.

The PID controller model [20, 21] was used to reproduce the desired heating rate. So the current passing through the system is described by the following equation:

$$I(t) = K_p \cdot e(t) + K_I \cdot \int_0^t e(\tau)\, d\tau + K_D \frac{de(t)}{dt}, \quad (3)$$

where $e(t)$ is the difference between the observed and calculated values of the temperature at the present time, K_P, K_I and K_D are the proportional, integral and differential coefficients, respectively.

The initial temperature of the system was equal to room temperature.

A convective heat sink was used as boundary conditions due to water cooling from the ends of the system, as well as heat losses on the opened surfaces due to radiation.

The first condition obeys the following equation:

$$q_c = h_c \left(T_s - T_0\right), \quad (4)$$

where h_c is the heat transfer coefficient, T_0 is the room temperature, T_s is the heat sink zone temperature.

The second boundary condition satisfies Stefan-Boltzmann law:

$$q_r = \sigma\epsilon \left(T^4 - T_0^4\right), \quad (5)$$

where σ is the Stefan-Boltzmann constant, ε is the absorptivity.

3. RESULTS

It was necessary to determine the temperature dependences of the thermal and electric resistances at the punch-matrix boundaries to complete the model. Basic experiments were carried out for these purposes to measure the temperature on the matrix surface, in its hole and various internal parts, including punches (15 mm in diameter), in the absence of thermal insulating felt. It was experimentally established that the key source of heat release to temperatures 1300-1400 °C is the contact resistance at the punch-matrix boundaries. Then the heat dissipation zone moves towards the punches. The data obtained helped to discover the thermal and electrical parameters of the contact resistance for the materials used in the mold, ensuring good coincidence of the observed and calculated figures of heat distribution at different temperatures.

A sintered aluminum oxide tablet was used as a sample during the experiments.

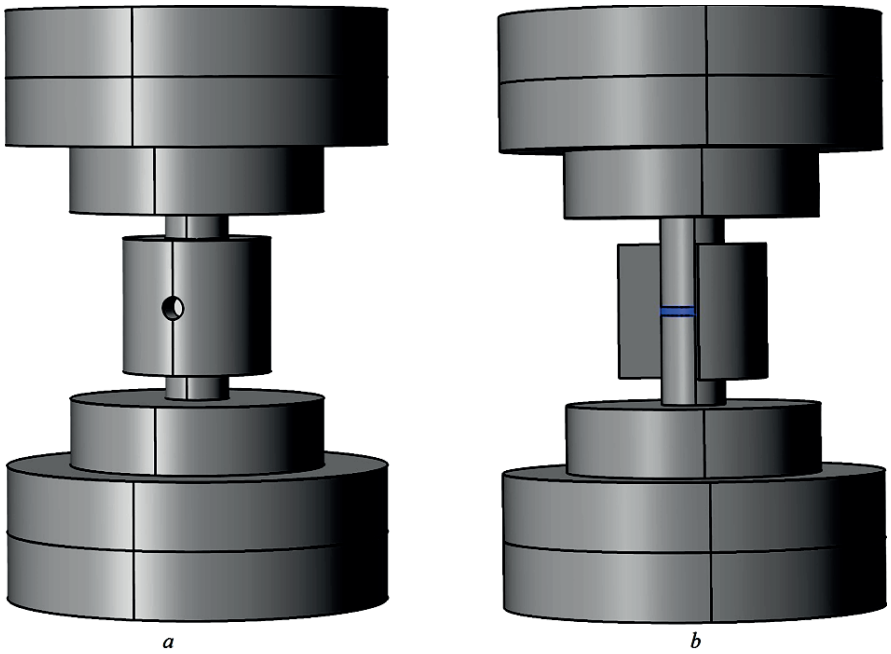

Figure 2: Schemes of the constructions for temperature measurement: *a* – hole of 5 mm in diameter and 8 mm in depth b - the matrix quarter was removed.

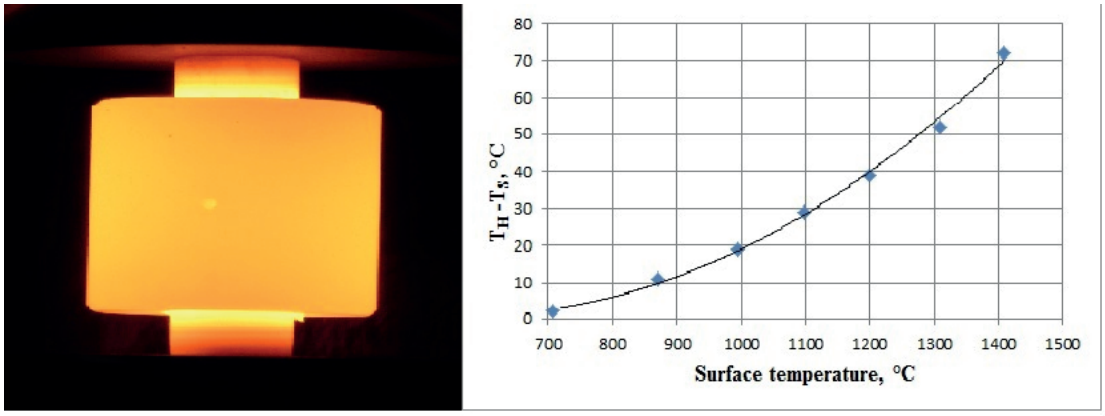

Figure 3: Photo of the mold and dependence of the difference between the hole and surface temperature on the surface temperature.

Figure 2 demonstrates designs of the construction used for temperature measurements. Experimental observations were based on the research results [7] and the temperature was measured by a thermal imager.

Figure 3 describes a photograph of the construction (Figure 2 (*a*)) at a surface temperature of 1000 °C, as well as a graph of the dependence of the difference between the hole temperature and the surface temperature on the mold surface temperature.

The figure demonstrates that as the surface temperature increases, the difference between the hole and surface temperatures behaves the same, that is quite expectable. However, it should be noted that in the absence of thermal insulation, the

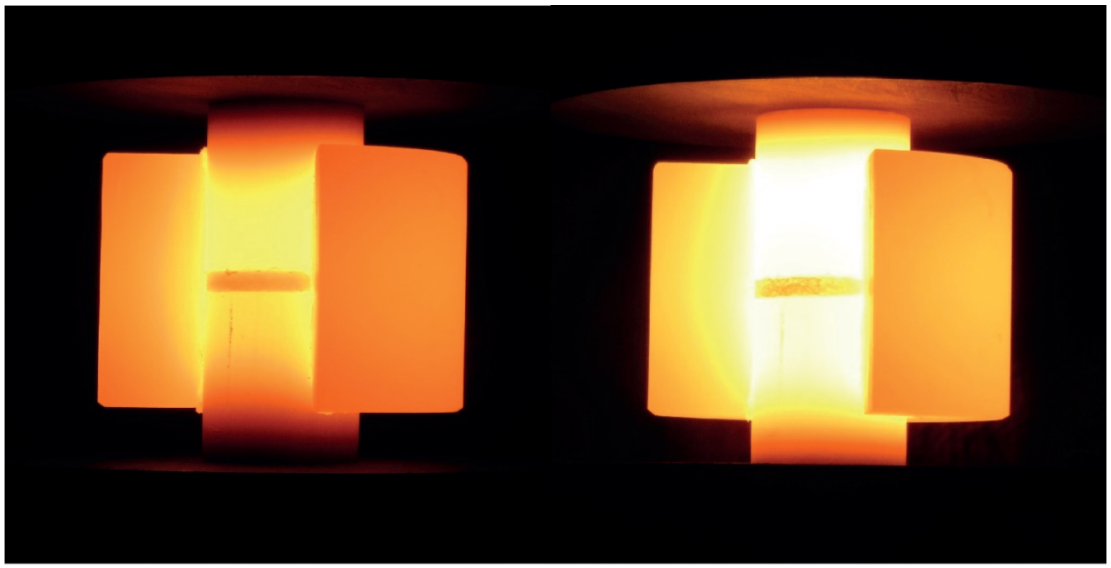

a *b*

Figure 4: Photographs of the mold at high and low surface temperatures: *a* - Surface temperature 1100 °C, *b* - Surface temperature 1500 °C.

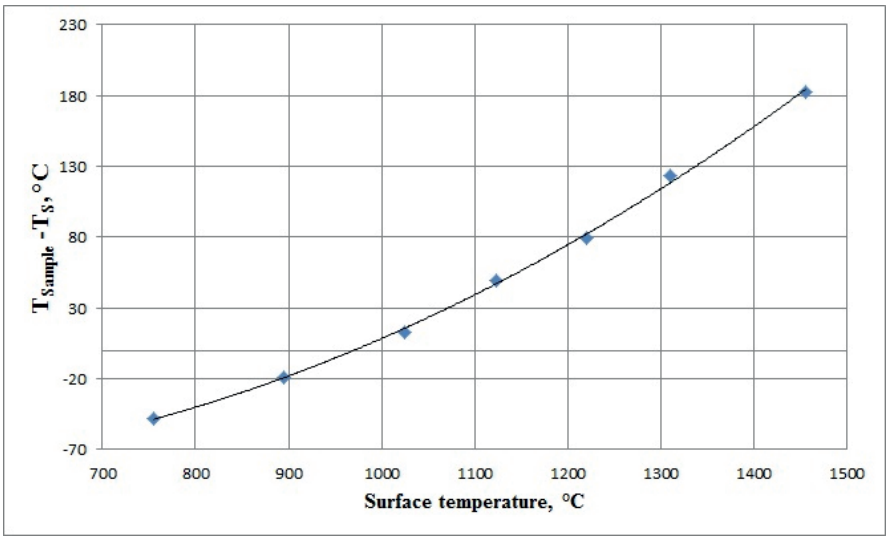

Figure 5: Graph of the dependence of the difference between the sample temperature and the surface temperature on the surface temperature.

results may be distorted. The felt presence will reduce the temperature difference, but the experiment scheme does not allow to clarify this point.

The next step was to determine how much the temperature differs between the surface and the sample. So the experiments were performed for the construction in Fig. 2 (*b*). Figure 4 shows photos of the mold at high and low temperatures, and Figure 5 - a graph of the dependence of the difference between the sample and surface temperatures on the surface temperature.

It turns out that the sample is colder than the surface is up to temperatures of 1000 °C. Moreover, there is one feature: the key source of heat release up to temperatures

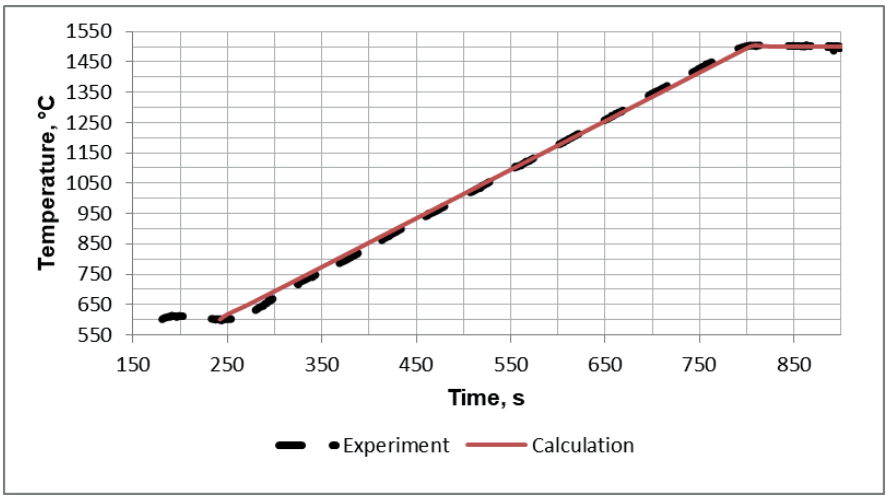

Figure 6: Graph of dependence of the matrix hole temperature on time for experimental and calculated data.

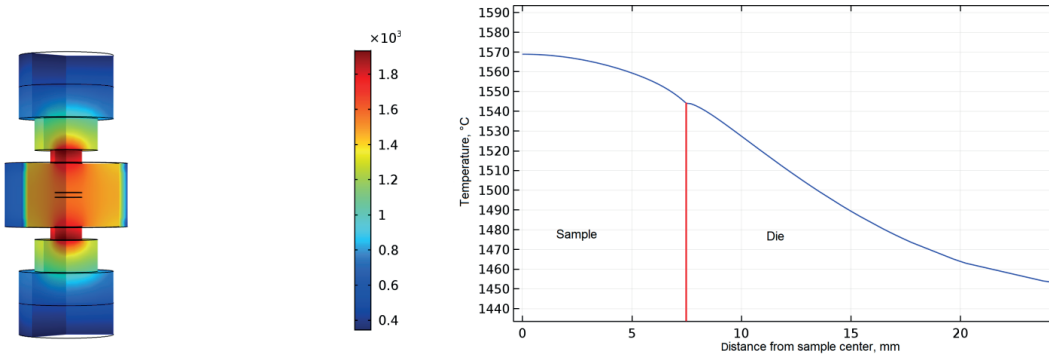

Figure 7: Temperature distribution in the volume of the system.

of 1300 - 1400 °C is the contact resistance at the boundaries of the punch-matrix. Then the heat dissipation zone moves towards the punches. Such a mechanism can be explained by the fact that while heating the thermal expansion of the punches occurs and results in the contact resistance lower.

Figure 6 describes a graph of the dependence of the matrix hole temperature on time for the experimental and calculated data for a heating rate of 100 °C / min, taking into account the thermal insulation. As the lower limit of measurements of the optical pyrometer is 600 °C, the data are compared for the values higher than this limit is.

As the figure shows, the simulation provides good coincidence with the experimental data.

Figure 7 shows the temperature distribution in the volume of the system during heating at the time before the isothermal holding begins, as well as the temperature distribution depending on the distance from the sample center.

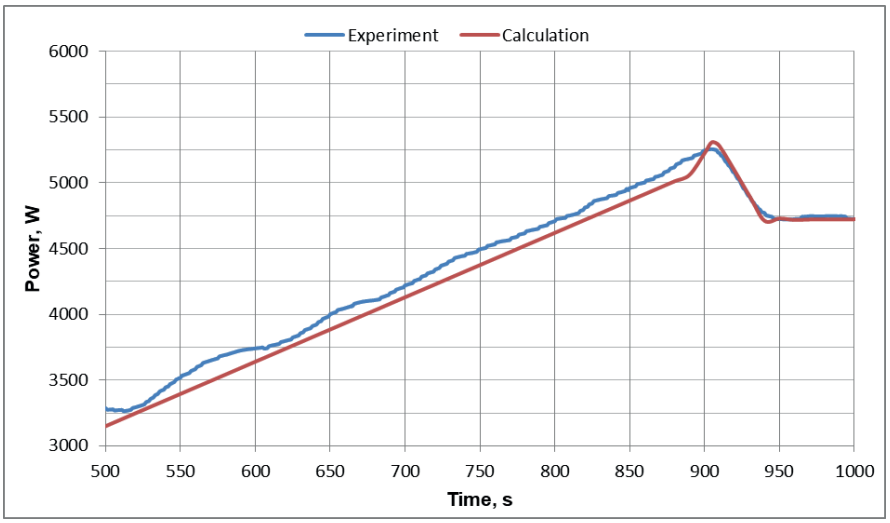

Figure 8: Dependence of the released power on time.

There is a temperature difference of about 120 °C between the sample center and the matrix surface. The temperature distribution in the volume of the system is consistent with the experimental data presented above.

For a more precise research of the model, it is necessary to compare the experimental and calculated data on the power released during sintering, as shown in Fig. 8.

The model provides a good coincidence with the experimental data. Differences in the values can be explained by the fact that the model does not take into account the power losses on the internal components of the installation.

4. DISCUSSIONS

The research experimental part feature is the discovery of the contact resistance at the punch-matrix boundaries as the main source of heat release up to temperatures of 1300-1400 °C. Then the heat dissipation zone moves towards the punches. Probably, this mechanism can be explained by the fact that during heating the thermal expansion of the punches happens and results in the contact resistance decreases. Moreover, the resistance of the contact itself decreases with temperature decrease.

The temperature of the sample to a certain point (1000 °C) is below the surface temperature. It can be presumed that this is a result of a more intensive heat removal due to radiation and thermal conductivity (to cooled electrodes) compared to its absorption in the sample.

The computational model showed a good agreement with the experiment, and its generalization to real systems with thermal insulation will let control the sample temperature through the surface or hole temperatures.

5. CONCLUSIONS

The experimental results let us understand a mechanism for the heat release source change. The source moves from the contacts to the punches. Such information is not available in the literature.

The temperature dependences of the thermal and contact resistances at the punch-matrix interface were figured out. The calculated model, constructed on these dependences, demonstrates good agreement with experiment.

The model was generalized to systems with thermal insulation and showed the possibility of controlling of the sample temperature by the surface or hole temperature. However, the heat-insulating felt usage reduces the temperature difference, but does not eliminate it.

The results can be generalized to any ceramic materials and geometric features of the installation.

ACKNOWLEDGMENT

The research was carried out within the state assignment of the Ministry of Education and Science of the Russian Federation (project No. 11.1957.2017/4.6).

References

[1] R. Orrù, R. Licheri, A.M. Locci, A. Cincotti, G. Cao, Consolidation/synthesis of materials by electric current activated/assisted sintering, Mater. Sci. Eng. R 63 (4–6) (2009) 127–287.

[2] O. Guillon, J.G. Julian, B. Dargatz, T. Kessel, G. Schierning, J. Räthel, M. Herrmann, Field-assisted sintering technology/spark plasma sintering: mechanisms, materials, and technology developments, Adv. Eng. Mater. 16 (7) (2014) 830–849.

[3] M. Suárez, A. Fernández, J.L. Menéndez, R. Torrecillas, H.U. Kessel, J. Hennicke, R. Kirchner, T. Kessel, Chapter 13: Challenges and opportunities for spark plasma sintering: a key technology for a new generation of materials, in: B. Ertuğ (Ed.), Sintering Applications, InTech, ISBN: 978-953-51-0974-7 2013, pp. 319–342

[4] Z.A. Munir, U. Anselmi-Tamburini, M. Ohyanagi, The effect of electric field and pressure on the synthesis and consolidation of materials: a review of the spark plasma sintering method, J. Mater. Sci. 41 (2006) 763–777.

[5] A. Pavia, L. Durand, F. Ajustron, V. Bley, G. Chevallier, A. Peigney, C. Estournès, Electro-thermal measurements and finite element method simulations of a spark plasma sintering device, J. Mater. Process. Technol. 213 (8) (2013) 1327–1336.

[6] L. Junting, S. Yan, Z. Chunxiang, Z. Zhiyong, Thermal-electrical coupled analysis and experimental investigation on spark plasma sintering of SiC ceramics, J. Wuhan Univ. Technol. - Mater. Sci. Ed. 27 (6) (2012) 1120–1124.

[7] C. Manière, A. Pavia, L. Durand, G. Chevallier, K. Afanga, C. Estournès Finite-element modeling of the electro-thermal contacts in the spark plasma sintering process, J. Eur. Ceram. Soc.,36 (2016) 741–748.

[8] A. Zavaliangos, J. Zhang, M. Krammer, J.R. Groza, Temperature evolution during field activated sintering, Mater. Sci. Eng. A 379 (1–2) (2004) 218–228.

[9] K. Vanmeensel, A. Laptev, J. Hennicke, J. Vleugels, O. Van der Biest, Modelling of the temperature distribution during field assisted sintering, Acta Mater. 53 (16) (2005) 4379–4388.

[10] X. Wang, S.R. Casolco, G. Xu, J.E. Garay, Finite element modeling of electric currentactivated sintering: the effect of coupled electrical potential, temperature and stress, Acta Mater. 55 (10) (2007) 3611–3622.

[11] B. McWilliams, A. Zavaliangos, Multi-phenomena simulation of electric field assisted sintering, J. Mater. Sci. 43 (14) (2008) 5031–5035.

[12] S. Muñoz, U. Anselmi-Tamburini, Temperature and stress fields evolution during spark plasma sintering processes, J. Mater. Sci. 45 (23) (2010) 6528–6539.

[13] P. Mondalek, L. Silva, M. Bellet, A numerical model for powder densification by SPS technique, Adv. Eng. Mater. 13 (7) (2011) 587–593.

[14] G. Antou, G. Mathieu, G. Trolliard, A. Maître, Spark plasma sintering of zirconium carbide and oxycarbide: finite element modeling of current density, temperature, and stress distributions, J. Mater. Res. 24 (02) (2009) 404–412.

[15] G. Maizza, S. Grasso, Y. Sakka, Moving finite-element mesh model for aiding spark plasma sintering in current control mode of pure ultrafine WC powder, J. Mater. Sci. 44 (5) (2009) 1219–1236.

[16] S. Muñoz, U. Anselmi-Tamburini, Parametric investigation of temperature distribution in field activated sintering apparatus, Int. J. Adv. Manuf. Technol. 65 (1) (2013) 127–140.

[17] Y. Achenani, M. Saâdaoui, A. Cheddadi, G. Bonnefont, G. Fantozzi, Finite element modeling of spark plasma sintering: Application to the reduction of temperature inhomogeneities, case of alumina, Materials and Design 116 (2017) 504–514.

[18] C. Maniere, A. Pavia, L. Durand, G. Chevallier, V. Bley, K. Afanga, A. Peigney, C. Estournes, Pulse analysis and electric contact measurements in spark plasma sintering, Electr. Power Syst. Res. 127 (2015) 307–313.

[19] E.A. Olevsky, C. Garcia-Cardona, W.L. Bradbury, C.D. Haines, D.G. Martin, D. Kapoor, Fundamental aspects of spark plasma sintering II: finite element analysis of scalability, J. Am. Ceram. Soc. 95 (2012) 2414–2422.

[20] A. Locci, A. Cincotti, S. Todde, R. Orrù and G, Cao, A methodology to investigate the intrinsic effect of the pulsed electric current during the spark plasma sintering of electrically conductive powders, Sci. Technol. Adv. Mater.11 (4) (2010) 045005.

[21] C. Maniere, G. Lee, E. Olevsky, Proportional integral derivative, modeling and ways of stabilization for the spark plasma sintering process, Results in Physics, 7 (2017) 1494 – 1497.